Sciencexpress Reports

# A near–quantum-limited Josephson traveling-wave parametric amplifier

**C. Macklin,[1,2]* K. O'Brien,[3] D. Hover,[4] M. E. Schwartz,[1] V. Bolkhovsky,[4] X. Zhang,[3,5,6] W. D. Oliver,[4,7] I. Siddiqi[1]**

[1]Quantum Nanoelectronics Laboratory, University of California, Berkeley, Berkeley, CA 94720, USA. [2]Computational Research Division, Lawrence Berkeley National Laboratory, Berkeley, CA 94720, USA. [3]Nanoscale Science and Engineering Center, University of California, Berkeley, Berkeley, CA 94720, USA. [4]MIT Lincoln Laboratory, 244 Wood Street Lexington, MA 02420, USA. [5]Materials Sciences Division, Lawrence Berkeley National Laboratory Berkeley, California 94720, USA. [6]Department of Physics, King Abdulaziz University, Jeddah 21589, Saudi Arabia. [7]Research Laboratory of Electronics, Massachusetts Institute of Technology 77 Massachusetts Avenue, Cambridge, MA 02139, USA.

*Corresponding author. E-mail: chris.macklin@berkeley.edu

**Detecting single photon level signals—carriers of both classical and quantum information—is particularly challenging for low-energy microwave frequency excitations. Here we introduce a superconducting amplifier based on a Josephson junction transmission line. Unlike current standing-wave parametric amplifiers, this traveling wave architecture robustly achieves high gain over a bandwidth of several gigahertz with sufficient dynamic range to read out 20 superconducting qubits. To achieve this performance, we introduce a sub-wavelength resonant phase matching technique that enables the creation of nonlinear microwave devices with unique dispersion relations. We benchmark the amplifier with weak measurements, obtaining a high quantum efficiency of 75% (70% including following amplifier noise). With a flexible design based on compact lumped elements, this Josephson amplifier has broad applicability to microwave metrology and quantum optics.**

Coherent superconducting circuits play a key role in exploring the interaction between light and matter at microwave frequencies, particularly at the level of single photons and artificial atoms where quantum effects dominate. Recent advances span quantum measurement (*1–4*), control (*5–7*), optics (*8*, *9*), and information processing (*10–12*). Many of these developments have relied on ultra-low-noise Josephson parametric amplifiers (JPAs) (*13–15*) to detect microwave frequency signals with a sensitivity approaching the minimum allowed by quantum mechanics (*16*). Although several refinements have been incorporated into JPAs (*17–20*), the basic architecture remains that of a cavity where anharmonicity is introduced via the nonlinear inductance of a Josephson junction. This architecture is well suited for detecting a few photons over a bandwidth of tens of megahertz; however, applications such as quantum computation and simulation with many bits motivate the development of a versatile, general purpose, quantum-limited microwave frequency amplifier with gigahertz-scale bandwidth and larger power handling capability. Semiconductor amplifiers based on high-electron-mobility transistors (HEMTs) fulfill some of these requirements, but generally achieve noise temperatures 10-20 times greater than the quantum limit.

We introduce a style of Josephson amplifier which sidesteps the primary limiting factor in JPAs - the use of a resonator to enhance the interaction between incident waves and the Josephson nonlinearity. Instead, we use a long chain of Josephson junctions, forming a metamaterial transmission line (*21*). We call this device a Josephson Traveling Wave Parametric Amplifier (JTWPA). The JTWPA does not have the fixed gain-bandwidth product intrinsic to resonant JPAs and can achieve power gain larger than 20 dB over a 3 GHz bandwidth. This performance is the result of a nonlinear phase-matching technique unique to the microwave domain that we call resonant phase matching (RPM), in which we manipulate the dispersion using an array of deep sub-wavelength resonators. The RPM technique could prove a fruitful tool in developing novel quantum optical devices at microwave frequencies.

Several features of the JTWPA make it attractive for a general-purpose ultra-low-noise cryogenic measurement system. The JTWPA does not inherently require a bulky, lossy microwave circulator at the input to separate incoming and outgoing modes. Furthermore, higher pump powers can be utilized in the JTWPA than in JPAs, enabling an order-of-magnitude increase in the input signal power that can be faithfully amplified. We measure noise performance of the JTWPA with a noise power technique and a fiducial quantum measurement, demonstrating a whole-system quantum efficiency of 49% - comparable to the most faithful JPAs. We utilize the JTWPA to make a projective qubit measurement to a fidelity of 96.7% in 100 ns at a measurement power 14 dB below the 1 dB compression power, implying the possibility of simultaneous readout of over 20 qubits. These factors make the JTWPA a more versatile measurement tool than the traditional JPA, providing the benefits of nearly quantum-limited performance with an ease of use comparable to a semiconductor amplifier. Traveling wave kinetic inductance amplifiers have recently been demonstrated (*22*, *23*), though an intense microwave drive of -10 dBm and a very long propagation length of 4.4 m are required for 20 dB gain, rendering integration with quantum information systems challenging.

The architecture of the JTWPA (Fig. 1) is a lumped-element transmission line utilizing a Josephson junction as

Downloaded from www.sciencemag.org on September 3, 2015

the inductive element, shunted to ground through a capacitor. The length of each unit cell is $a = 16$ $\mu$m; the device presented here comprises 2037 unit cells for a propagation length of 3.3 cm. The devices are fabricated in a niobium trilayer process on silicon (*24*, *25*). We have presented a theoretical treatment of the JTWPA in Ref. (*21*). When a strong microwave pump wave propagates down the line, the nonlinear inductance of the junctions permits four-wave mixing. Efficient parametric amplification requires the waves at the pump ($\omega_p$), signal ($\omega_s$), and idler ($\omega_i$) frequencies to satisfy energy conservation, $2\omega_p = \omega_s + \omega_i$, and momentum conservation (or, equivalently, phase matching), $\Delta k = 2k_p - k_s - k_i = 0$ where k is the wavevector. The former is satisfied by the creation of the idler at $\omega_i$, but the latter is only satisfied for certain dispersion relations $k(\omega)$.

For small signals, $k(\omega)$ is approximately a linear function of frequency and $\Delta k \approx 0$. However, when the line is strongly driven, the pump wave induces additional power-dependent phase shifts (*26*). In the case of the JTWPA, this shift is well approximated by

$$\Delta k = 2k_p - k_s - k_i - 2k_p\kappa_{nl} \quad (1)$$

where $\kappa_{nl} = (a^2 k_p^2 |Z|^2 / 16 L^2 \omega_p^2)(I_p / I_0)^2$, $Z$ is the characteristic impedance, $L$ is the Josephson inductance, and $I_p / I_0$ is the ratio of the pump current to the junction critical current (*21*). To satisfy this relation, we introduce the RPM technique: we add a series of linear lumped-element resonators (Fig. 1A), creating a stop band near 7.25 GHz. Nearby but outside the stop band wave propagation is unchanged aside from a small increase in $k(\omega)$. Choosing a pump frequency in this region provides the necessary increase in $k_p$ to partially compensate the power-dependent term in Eq. 1.

The setup for measuring amplifier gain is depicted in Fig. 2A. All measurements take place in a dilution refrigerator with a base temperature of 30 mK. We measure a 1 dB insertion loss for the JTWPA in the small-signal regime at 4 GHz, smoothly increasing to 4 dB at 10 GHz, in good agreement with capacitive dielectric loss (fig. S3). The RPM stop band is visible as a dip in transmission at 7.25 GHz (Fig. 2B).

The effect of RPM on the phase mismatch $\Delta k$ is shown in Fig. 2C. For a pump far from the dispersion feature, $\Delta k \sim 0$ in the weak-pump regime, and becomes poorly phase-matched as the pump power is increased. For a pump near the dispersion feature, the phase matching is sufficiently improved to realize a significant enhancement in gain. We focus here on one operating condition, with a pump at 7.157 GHz and $I_p / I_0 = 0.91$; the resulting gain profile is shown in Fig. 2D. This represents the most general-purpose operating configuration, with 20 dB of gain over a 3 GHz bandwidth.

We use a circuit quantum electrodynamics (QED) system (*27*) in the weak measurement limit to assess the noise performance of the JTWPA. By measuring the system parameters and utilizing the AC Stark shift of the qubit to calibrate the dispersive shift $\chi$ and the mean photon number occupation of the cavity $\bar{n}$, we extract a precisely calibrated power at the output of the cavity as $P = \kappa\hbar\omega_r\bar{n}$ where $\kappa$ and $\omega_r$ are the cavity's linewidth and frequency. This technique yields the system noise temperature at the reference plane relevant to quantum measurement with no additional uncertainty. This is a significant improvement over cryogenic power references which require additional components between the calibration device and the measurement reference plane (*28*, *29*), resulting in uncertainties in extracted system noise temperatures of 1 to 2 dB (*20*, *30*).

A simplified schematic for this measurement is shown in Fig. 3A. The qubit and cavity are of the "3D Transmon" variety (*31*); the single-junction Transmon qubit has a fixed frequency $\omega_{qb} / 2\pi = 3.58$ GHz and is antenna-coupled to an aluminum waveguide cavity with a resonant frequency $\omega_r / 2\pi = 5.984$ GHz and output coupling rate $\kappa / 2\pi = 18.5$ MHz. We measure the dispersive coupling rate to be $\chi / 2\pi = 584 \pm 5$ kHz. For additional details, see (*25*). Noise power spectra taken of the output microwave field in the vicinity of the cavity frequency are shown in Fig. 3B. A coherent tone corresponding to a mean cavity occupation $\bar{n} = 3.62 \pm 0.04$ allows us to directly refer the measured spectra to the output plane of the cavity. With the JTWPA pump off we extract a system noise of $9.01 \pm 0.23$ K. We turn the pump on and measure a signal gain of 21.6 dB; we refer the resulting noise level to the cavity output by subtracting this gain from the measured trace, permitting a direct comparison of noise temperature. We measure a system noise of $602 \pm 15$ mK, equivalent to a quantum measurement efficiency $\eta = \dfrac{\hbar\omega_r}{k_b T_{sys}} = 0.48 \pm 0.016$.

Several factors contribute to the measured reduction in $\eta$ from 1, including insertion loss in the microwave network between the cavity and JTWPA ($\eta_L = 0.69$), distributed loss in the JTWPA itself ($\eta_D = 0.9$), and the finite gain of the JTWPA compared to the HEMT noise ($\eta_H = 0.93$) (*25*). If we calculate $\eta = \eta_L \cdot \eta_H \cdot \eta_D \cdot \eta_J$, where $\eta_J$ is an extra factor we attribute to unaccounted inefficiency in amplifier operation, we extract the intrinsic quantum efficiency of the JTWPA to be $\eta_D \cdot \eta_J = 0.75$. The signal power calibration also allows us to directly assess the dynamic range of the TWPA. We measure 1 dB gain compression at an input power of -99 dBm (fig. S9), about 7 to 10 dB higher than demonstrated in any resonator-based JPAs with comparable gain (*8*, *20*).

We make an independent assessment of the quantum efficiency using the results for dephasing in a circuit QED measurement (*32*). In the limit relevant to weak measurement, the dephasing rate is given by $\Gamma_m = 8\chi^2\bar{n} / \kappa$. The rate

of qubit state information collection is related to the signal-to-noise ratio (SNR) of integrated readout histograms as $\Gamma_m^{'} = (SNR)^2 / 8\tau$ where $\tau$ is the measurement integration time. The quantum efficiency is the ratio of these two quantities, $\eta = \Gamma_m^{'} / \Gamma_m$, which saturates to 1 when the dephasing rate and the rate of information collection are equal (*33*).

The control sequence for this measurement is shown in Fig. 3C. We use heralding to post-select a pure ground state ensemble (*34*). We prepare half of the ensemble in $|1\rangle$ by applying a $\pi$-pulse and leave the other half in $|0\rangle$, followed by a weak measurement of variable amplitude. A final strong measurement allows the use of post-selection to eliminate records that underwent an undesired state transition. We integrate the weak measurement for a variable time and histogram the results, fit the histograms for the $|0\rangle$ and $|1\rangle$ sub-ensembles to Gaussian functions, and extract the SNR. Example histograms are shown in Fig. 3D for $\bar{n} = 3.62$ and $\tau = 1$ $\mu$s. We repeat this experiment for a range $\bar{n}$ from 0.3 to 3.6 and $\tau$ from 1 to 4.6 $\mu$s, extracting a mean quantum efficiency $\eta = 0.49 \pm 0.01$, in excellent agreement with the result obtained from the noise power method.

To test the performance of the JTWPA in a high-fidelity projective measurement, we exchange the weak-measurement-optimized qubit and cavity for another pair more optimized for strong measurement, with $\chi / 2\pi = 2.2$ MHz and $\kappa / 2\pi = 8.7$ MHz. The control sequence for projective readout is the same as in Fig. 3C except for the absence of the weak measurement. Using $\bar{n} = 23.3$ and a 100 ns integration window, we measure well-separated readout histograms shown in Fig. 4A. We extract a raw measurement fidelity $F = 1 - P_{1|0} - P_{0|1} = 0.967$ where $P_{a|b}$ is the probability of identifying the qubit state as $|a\rangle$ when it was prepared as $|b\rangle$.

The error is dominated by relaxation of the qubit and and spurious excitation between the heralding readout and the final readout, contributing about 0.026 and 0.007, respectively. Based on Gaussian fits to the state histograms, the intrinsic overlap of the histograms contributes about $10^{-5}$ of the total measurement error. The readout error due to histogram overlap associated with the quantum efficiency is plotted versus readout power and $\bar{n}$ in Fig. 4B. The readout power needed to achieve a $10^{-5}$ error level is 14 dB below the 1 dB compression power of the JTWPA, implying that over 20 qubits could be simultaneously read out without a degradation in performance. The prospect of multiplexing so many qubits onto a single readout line is important progress toward a scalable readout architecture for a quantum computer based on superconducting qubits. Further improvements in the dynamic range of the JTWPA leveraging Josephson junction arrays could enable even greater multiplexing ability.

The large bandwidth and power handling ability of the JWTPA are well-suited toward a variety of detector applications. Additionally, such an amplifier provides a resource for microwave quantum optics with the possibility of generating broadband or multi-mode squeezed radiation. The inherent transmission geometry may reduce or eliminate the need for intermediate isolators if the passive microwave embedding environment is carefully engineered. The low-loss deep-subwavelength loading structures used in RPM would be challenging or impossible to implement in optical-frequency systems, enabling a rich landscape of phase-matched nonlinear microwave circuits.

## REFERENCES AND NOTES


1. S. J. Weber, A. Chantasri, J. Dressel, A. N. Jordan, K. W. Murch, I. Siddiqi, Mapping the optimal route between two quantum states. *Nature* **511**, 570–573 (2014). Medline doi:10.1038/nature13559
2. N. Roch, M. E. Schwartz, F. Motzoi, C. Macklin, R. Vijay, A. W. Eddins, A. N. Korotkov, K. B. Whaley, M. Sarovar, I. Siddiqi, Observation of measurement-induced entanglement and quantum trajectories of remote superconducting qubits. *Phys. Rev. Lett.* **112**, 170501 (2014). Medline doi:10.1103/PhysRevLett.112.170501
3. P. Campagne-Ibarcq, L. Bretheau, E. Flurin, A. Auffèves, F. Mallet, B. Huard, Observing interferences between past and future quantum states in resonance fluorescence. *Phys. Rev. Lett.* **112**, 180402 (2014). Medline doi:10.1103/PhysRevLett.112.180402
4. M. Hatridge, S. Shankar, M. Mirrahimi, F. Schackert, K. Geerlings, T. Brecht, K. M. Sliwa, B. Abdo, L. Frunzio, S. M. Girvin, R. J. Schoelkopf, M. H. Devoret, Quantum back-action of an individual variable-strength measurement. *Science* **339**, 178–181 (2013). Medline doi:10.1126/science.1226897
5. R. Vijay, C. Macklin, D. H. Slichter, S. J. Weber, K. W. Murch, R. Naik, A. N. Korotkov, I. Siddiqi, Stabilizing Rabi oscillations in a superconducting qubit using quantum feedback. *Nature* **490**, 77–80 (2012). Medline doi:10.1038/nature11505
6. G. de Lange, D. Ristè, M. J. Tiggelman, C. Eichler, L. Tornberg, G. Johansson, A. Wallraff, R. N. Schouten, L. DiCarlo, Reversing quantum trajectories with analog feedback. *Phys. Rev. Lett.* **112**, 080501 (2014). doi:10.1103/PhysRevLett.112.080501
7. S. Shankar, M. Hatridge, Z. Leghtas, K. M. Sliwa, A. Narla, U. Vool, S. M. Girvin, L. Frunzio, M. Mirrahimi, M. H. Devoret, Autonomously stabilized entanglement between two superconducting quantum bits. *Nature* **504**, 419–422 (2013). Medline doi:10.1038/nature12802
8. C. Eichler, Y. Salathe, J. Mlynek, S. Schmidt, A. Wallraff, Quantum-limited amplification and entanglement in coupled nonlinear resonators. *Phys. Rev. Lett.* **113**, 110502 (2014). Medline doi:10.1103/PhysRevLett.113.110502
9. E. Flurin, N. Roch, F. Mallet, M. H. Devoret, B. Huard, Generating entangled microwave radiation over two transmission lines. *Phys. Rev. Lett.* **109**, 183901 (2012). Medline doi:10.1103/PhysRevLett.109.183901
10. R. Barends, J. Kelly, A. Megrant, A. Veitia, D. Sank, E. Jeffrey, T. C. White, J. Mutus, A. G. Fowler, B. Campbell, Y. Chen, Z. Chen, B. Chiaro, A. Dunsworth, C. Neill, P. O'Malley, P. Roushan, A. Vainsencher, J. Wenner, A. N. Korotkov, A. N. Cleland, J. M. Martinis, Superconducting quantum circuits at the surface code threshold for fault tolerance. *Nature* **508**, 500–503 (2014). Medline doi:10.1038/nature13171
11. D. Ristè, S. Poletto, M. Z. Huang, A. Bruno, V. Vesterinen, O. P. Saira, L. DiCarlo, Detecting bit-flip errors in a logical qubit using stabilizer measurements. *Nat. Commun.* **6**, 6983 (2015). Medline doi:10.1038/ncomms7983
12. J. M. Chow, J. M. Gambetta, E. Magesan, D. W. Abraham, A. W. Cross, B. R. Johnson, N. A. Masluk, C. A. Ryan, J. A. Smolin, S. J. Srinivasan, M. Steffen, Implementing a strand of a scalable fault-tolerant quantum computing fabric. *Nat. Commun.* **5**, 4015 (2014). Medline doi:10.1038/ncomms5015
13. M. A. Castellanos-Beltran, K. W. Lehnert, Widely tunable parametric amplifier based on a superconducting quantum interference device array resonator. *Appl. Phys. Lett.* **91**, 083509 (2007). doi:10.1063/1.2773988
14. N. Bergeal, F. Schackert, M. Metcalfe, R. Vijay, V. E. Manucharyan, L. Frunzio, D. E. Prober, R. J. Schoelkopf, S. M. Girvin, M. H. Devoret, Phase-preserving

amplification near the quantum limit with a Josephson ring modulator. *Nature* **465**, 64–68 (2010). Medline doi:10.1038/nature09035
15. M. Hatridge, R. Vijay, D. H. Slichter, J. Clarke, I. Siddiqi, Dispersive magnetometry with a quantum limited SQUID parametric amplifier. *Phys. Rev. B* **83**, 134501 (2011). doi:10.1103/PhysRevB.83.134501
16. C. Caves, Quantum limits on noise in linear amplifiers. *Phys. Rev. D Part. Fields* **26**, 1817–1839 (1982). doi:10.1103/PhysRevD.26.1817
17. T. Yamamoto, K. Inomata, M. Watanabe, K. Matsuba, T. Miyazaki, W. D. Oliver, Y. Nakamura, J. S. Tsai, Flux-driven Josephson parametric amplifier. *Appl. Phys. Lett.* **93**, 042510 (2008). doi:10.1063/1.2964182
18. N. Roch, E. Flurin, F. Nguyen, P. Morfin, P. Campagne-Ibarcq, M. H. Devoret, B. Huard, Widely tunable, nondegenerate three-wave mixing microwave device operating near the quantum limit. *Phys. Rev. Lett.* **108**, 147701 (2012). Medline doi:10.1103/PhysRevLett.108.147701
19. C. Eichler, A. Wallraff, Controlling the dynamic range of a Josephson parametric amplifier. *EPJ Quantum Technology* **1**, 2 (2014). doi:10.1140/epjqt2
20. J. Y. Mutus, T. C. White, R. Barends, Y. Chen, Z. Chen, B. Chiaro, A. Dunsworth, E. Jeffrey, J. Kelly, A. Megrant, C. Neill, P. J. J. O'Malley, P. Roushan, D. Sank, A. Vainsencher, J. Wenner, K. M. Sundqvist, A. N. Cleland, J. M. Martinis, Strong environmental coupling in a Josephson parametric amplifier. *Appl. Phys. Lett.* **104**, 263513 (2014). doi:10.1063/1.4886408
21. K. O'Brien, C. Macklin, I. Siddiqi, X. Zhang, Resonant phase matching of Josephson junction traveling wave parametric amplifiers. *Phys. Rev. Lett.* **113**, 157001 (2014). Medline doi:10.1103/PhysRevLett.113.157001
22. B. Ho Eom, P. K. Day, H. G. LeDuc, J. Zmuidzinas, A wideband, low-noise superconducting amplifier with high dynamic range. *Nat. Phys.* **8**, 623–627 (2012). doi:10.1038/nphys2356
23. C. Bockstiegel, J. Gao, M. R. Vissers, M. Sandberg, S. Chaudhuri, A. Sanders, L. R. Vale, K. D. Irwin, D. P. Pappas, Development of a broadband NbTiN traveling wave parametric amplifier for MKID readout. *J. Low Temp. Phys.* **176**, 476–482 (2014). doi:10.1007/s10909-013-1042-z
24. S. K. Tolpygo *et al.*, *IEEE Trans. Appl. Supercond.* **25**, 1101312 (2015).
25. Materials and methods are available as supplementary materials on *Science* Online.
26. G. P. Agrawal, *Nonlinear Fiber Optics* (Academic Press, 2012), fifth edn.
27. A. Blais, R.-S. Huang, A. Wallraff, S. M. Girvin, R. J. Schoelkopf, Cavity quantum electrodynamics for superconducting electrical circuits: An architecture for quantum computation. *Phys. Rev. A* **69**, 062320 (2004). doi:10.1103/PhysRevA.69.062320
28. J. E. Fernandez, "A Noise Measurement System Using a Cryogenic Attenuator," *TMO Prog. Rep.* **42-135** (1998).
29. L. Spietz, K. W. Lehnert, I. Siddiqi, R. J. Schoelkopf, Primary electronic thermometry using the shot noise of a tunnel junction. *Science* **300**, 1929–1932 (2003). Medline doi:10.1126/science.1084647
30. M. A. Castellanos-Beltran, K. D. Irwin, G. C. Hilton, L. R. Vale, K. W. Lehnert, Amplification and squeezing of quantum noise with a tunable Josephson metamaterial. *Nat. Phys.* **4**, 929–931 (2008). doi:10.1038/nphys1090
31. H. Paik, D. I. Schuster, L. S. Bishop, G. Kirchmair, G. Catelani, A. P. Sears, B. R. Johnson, M. J. Reagor, L. Frunzio, L. I. Glazman, S. M. Girvin, M. H. Devoret, R. J. Schoelkopf, Observation of high coherence in Josephson junction qubits measured in a three-dimensional circuit QED architecture. *Phys. Rev. Lett.* **107**, 240501 (2011). Medline doi:10.1103/PhysRevLett.107.240501
32. M. Boissonneault, J. M. Gambetta, A. Blais, Dispersive regime of circuit QED: Photon-dependent qubit dephasing and relaxation rates. *Phys. Rev. A* **79**, 013819 (2009). doi:10.1103/PhysRevA.79.013819
33. A. Korotkov, Selective quantum evolution of a qubit state due to continuous measurement. *Phys. Rev. B* **63**, 115403 (2001). doi:10.1103/PhysRevB.63.115403
34. J. E. Johnson, C. Macklin, D. H. Slichter, R. Vijay, E. B. Weingarten, J. Clarke, I. Siddiqi, Heralded state preparation in a superconducting qubit. *Phys. Rev. Lett.* **109**, 050506 (2012). Medline doi:10.1103/PhysRevLett.109.050506

## ACKNOWLEDGMENTS

We acknowledge A. Kamal, S. Tolpygo and G. Fitch for useful discussions and technical assistance. C.M. acknowledges E. Hassell and J. Luke for useful discussions. This research is based upon work supported in part by the Army Research Office (ARO) under Grant No. W911NF-14-1-0078; the Office of the Director of National Intelligence (ODNI), Intelligence Advanced Research Projects Activity (IARPA), via MIT Lincoln Laboratory under Air Force Contract FA8721-05-C-0002; and a Multidisciplinary University Research Initiative from the Air Force Office of Scientific Research (AFOSR MURI Grant No. FA9550-12-1-0488). The views and conclusions contained herein are those of the authors and should not be interpreted as necessarily representing the official policies or endorsements, either expressed or implied, of ODNI, IARPA, or the U.S. Government. The U.S. Government is authorized to reproduce and distribute reprints for Governmental purpose notwithstanding any copyright annotation thereon. M.E.S. acknowledges support from a Hertz Foundation Fellowship.

## SUPPLEMENTARY MATERIALS

www.sciencemag.org/cgi/content/full/science.aaa8525/DC1
Materials and Methods
Figs. S1 to S12

5 February 2015; accepted 19 August 2015
Published online 3 September 2015
10.1126/science.aaa8525

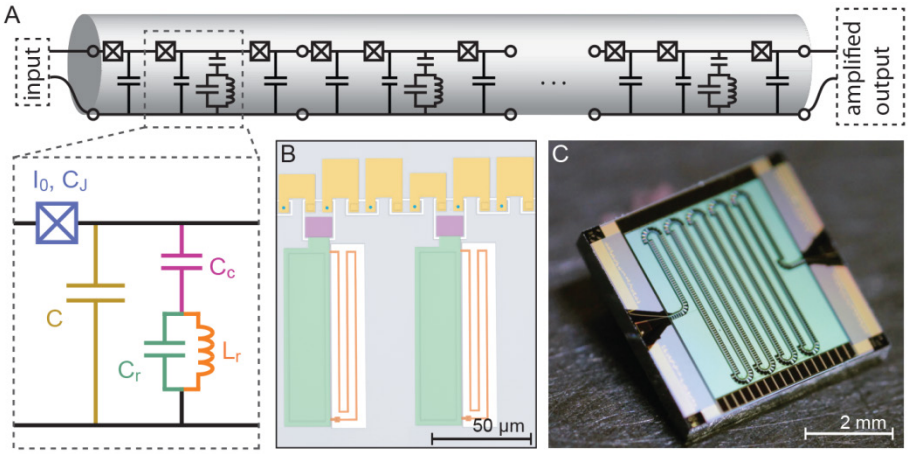


**Fig. 1. Josephson traveling-wave parametric amplifier.** (**A**) Circuit diagram. The JTWPA is implemented as a nonlinear lumped-element transmission line; one unit cell consists of a Josephson junction with critical current $I_0 = 4.6$ $\mu$A and intrinsic capacitance $C_J = 55$ fF with a capacitive shunt to ground $C = 45$ fF. Every third unit cell includes a lumped-element resonator designed with capacitance $C_r = 6$ pF and inductance $L_r$ = 120 pH, with coupling strength set by a capacitor $C_c = 20$ fF. The value of $C$ in the resonator-loaded cell is reduced to compensate for the addition of $C_c$. (**B**) False-color optical micrograph. The coloring corresponds to the inset in **A**, with the lower metal layer shown in gray. (**C**) Photograph of a 2037 junction JTWPA. The line is meandered several times on the 5 mm × 5 mm chip to achieve the desired amplifier gain.

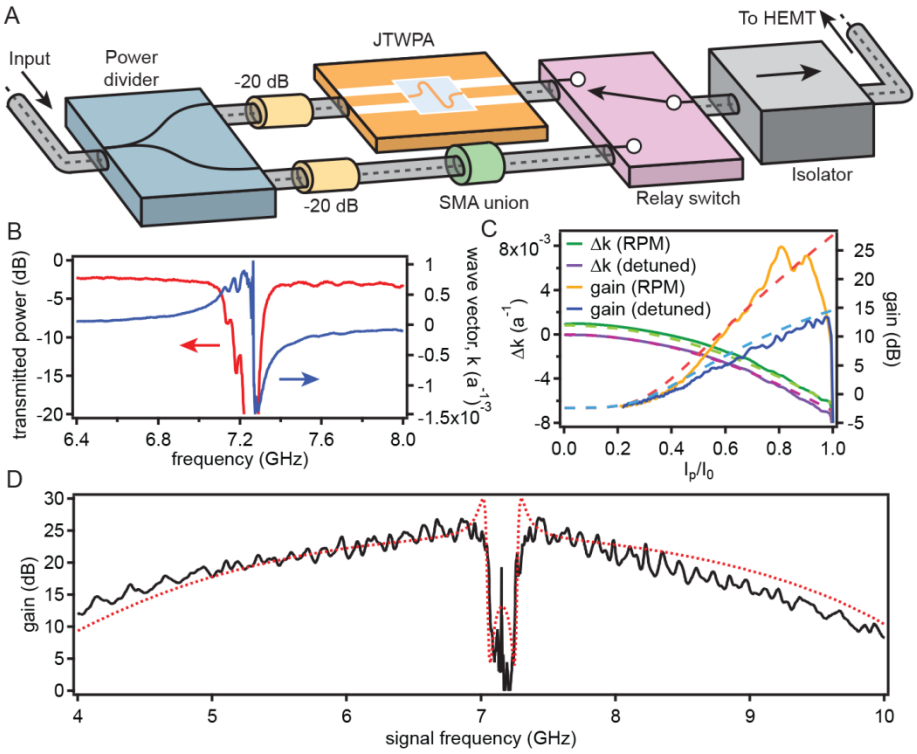


**Fig. 2. Resonant phase matching.** (**A**) Cryogenic transmission calibration setup. Input signals are split using a power divider followed by a 20 dB attenuator. We connect a JTWPA to one arm and a microwave union to the other arm using identical microwave cables. A switch selects which measurement chain is connected to the HEMT amplifier. (**B**) Small-signal transmission of the JTWPA, showing the transmission dip (red) and wave vector shift (blue) due to the dispersion feature near 7.25 GHz. The small ripples are due to inhomogeneity in the frequency of the RPM resonators. (**C**) Phase mismatch and gain. The phase mismatch $\Delta k$ is shown for a pump at 7.157 GHz (solid green, "RPM") and at 6.5 GHz (solid purple, "detuned") versus pump power, with a signal at 6.584 GHz. The decrease in $|\Delta k|$ at large pump power for the RPM case corresponds to an enhancement in the gain (solid gold) compared to a detuned pump (solid blue). Theory overlays are shown as dashed lines in complementary colors. The measured gain curve slumps due to a drop in pump transmission for pump currents near the junction critical current. Improvements to the RPM resonators could enable further enhancement of gain. (**D**) Gain profile of the JTWPA with a strong pump applied at 7.157 GHz and $I_p / I_0 = 0.91$. The ripples are due to imperfect impedance matching between the JTWPA and the embedding environment. A predicted gain profile (dotted red) is overlaid, in good agreement with the measured performance.

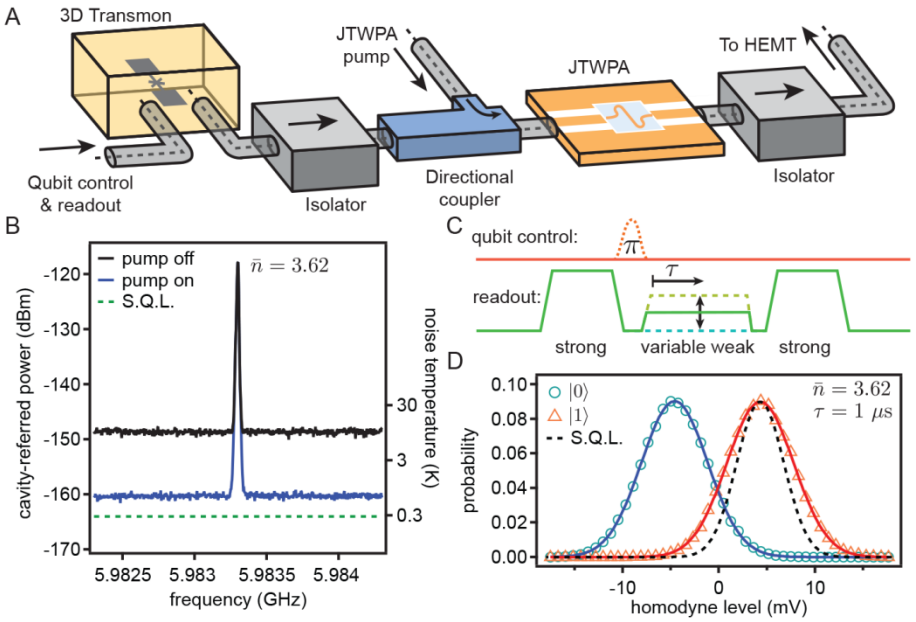


**Fig. 3. Noise performance of JTWPA.** (**A**) Cryogenic circuit schematic. Readout and control pulses enter the 3D transmon system at left. The transmitted readout signal leaves through the strongly coupled port at right. The pump tone for the JTWPA enters via a directional coupler. (**B**) Calibrated noise spectra. The known signal power calibrates the spectra to the cavity output plane. Using a measurement bandwidth of 10 kHz, we extract the system noise on the right axis. With the pump on (blue trace), we find a system noise of $2.10 \pm 0.05$ times the standard quantum limit (green dashes). (**C**) Pulse sequence for weak measurement. An initial strong measurement heralds the ground state. The qubit is then prepared in the excited state or left in the ground state. A variable-strength weak measurement is applied, followed by a final strong measurement. (**D**) Example weak measurement histograms with $\bar{n} = 3.62$ and $\tau = 1$ $\mu$s with Gaussian fits. The black dashed line illustrates the histogram width expected for a fully quantum-limited measurement.

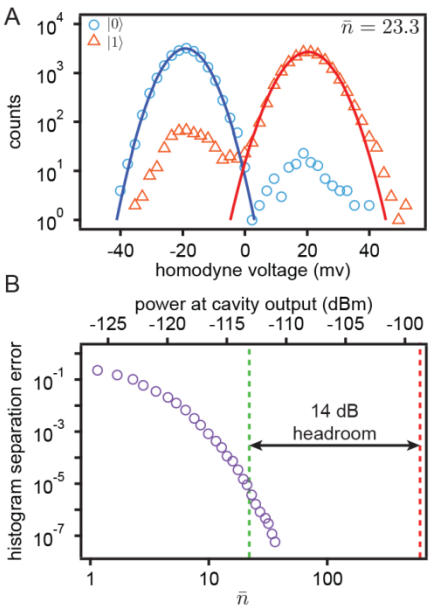


**Fig. 4. High-fidelity projective measurement.** (**A**) Optimized projective readout histograms. The intrinsic overlap of the histograms contributes less than $10^{-5}$ of the total error. (**B**) Histogram separation error for 100 ns integration window. The measurement power required to achieve a histogram separation error below $10^{-5}$ (dashed green line) is 14 dB below the measured 1 dB compression power of the JTWPA (dashed red line).